



DEGRADATION BEHAVIOR BY LOCAL BUCKLING AND/OR FRACTURE OF H-SHAPED STEEL BEAM WITH AXIAL DEFORMATION RESTRAINED

Y. Koetaka⁽¹⁾, R. Murakami⁽²⁾

⁽¹⁾ Associate Professor, Kyoto University, koetaka@archi.kyoto-u.ac.jp

⁽²⁾ Staff, Nikken Sekkei, LTD., murakami.ryuto@nikken.jp

Abstract

Against quite huge earthquakes, steel moment frames may collapse completely as resisting capacities of steel members decrease by occurring local buckling, lateral-torsional buckling or fracture. In previous numerical studies on the steel moment frames considering the degradation behaviors of steel members, the collapse behavior of the frames under quite huge earthquakes was examined. Most of these researches adopted rotational spring models for beams, based on the idea that axial force didn't act on the beams. On the other hand, steel beams in moment frames are restrained from the axial deformation by other beams, columns, and floor slab. Although it is considered that the degradation behavior of beams is affected by such axial deformation restriction, there are a few studies on the degradation behavior of beams after occurring only lateral-torsional buckling. In this paper, the effect of axial deformation restriction on the degradation behavior of H-shaped steel beams after local buckling and/or fracture occurring is revealed.

First, cyclic loading test was conducted to clarify differences of hysteresis characteristics of H-shaped steel beams by the axial deformation restriction after local buckling and/or fracture occur. The test specimen consists of a welded H-shaped steel beam and a square hollow section column, and they are connected by through-diaphragms. Test parameters are width-to-thickness ratios of web and flange of the beam, the presence or absence of weld access holes at the end of the beam, and the presence or absence of axial deformation restriction. As an experimental result, it was clarified that out-of-plane deformation of flange due to local buckling becomes smaller and strength decreased more slowly after occurring local buckling in case of the beams with axial deformation restriction. Furthermore, it was revealed the magnitude of axial deformation restriction didn't affect the timing of crack initiation if strength degradation by local buckling was not remarkable.

Secondly, to examine a range of axial deformation restriction that influences the degradation behavior due to local buckling of beams, finite element analysis (FEA) was conducted varying the magnitude of axial deformation restriction. Considering characteristics of the degradation behavior through FEA results, the axial deformation restriction can be classified into three ranges using a ratio of rigidity of the frame to axial rigidity of the beam (k_f/k_b). The degradation behavior due to local buckling of beams with small axial restriction ($k_f/k_b < 0.01$) was identical to that of the beam with no axial restriction. In this range, it is considered that a rotational spring model can be applied for beams on even the complete collapse analysis of frames. On the other hand, the behavior of beams with large axial restriction ($k_f/k_b > 1$) indicated the same as that of the beam completely restricted. When the axial restriction was moderate ($0.01 < k_f/k_b < 1$), the degradation behavior was intermediate between these ranges. As a result, it would be better to adopt the numerical model considering the axial deformation of beams in case of the latter two ranges ($k_f/k_b > 0.01$) for the complete collapse analysis.

Keywords: H-shaped steel beam, Axial deformation restriction, Local buckling, Fracture, Degradation behavior



1. Introduction

During quite huge earthquakes, local buckling, lateral-torsional buckling and/or fracture of steel members may occur, in the worst case, the steel moment-resisting frames may collapse completely due to the strength degradation of steel members. To update the seismic design code on the strong seismic regions for saving the structures from such serious damages, we should understand the ultimate state of the structures until complete collapse with the accuracy as high as possible.

By now, complete collapse analysis has been conducted using a numerical model that is considered with the strength degradation of steel members (see Ref. [1] to [6]). In some studies, spring models possessing only rotational degree have been adopted to trace the strength degradation of beams. The hysteresis rules of the spring model have modeled based on the experimental studies of cantilever type whose axial deformation was free (for example, Ref. [7] to [9], etc.).

However, axial deformations of the beams at the moment-resisting frames are restricted by the adjacent members, e.g., beams, columns, and floor slab, thus it is considered that the strength degradation and ultimate state of the beam are influenced by the axial restriction. Regarding such a research subject, Kanao et al. [10], Nakata et al. [11], and Iga et al. [12] mentioned that the strength degradation after lateral-torsional buckling occurring became milder because of the axial deformation restriction. Meanwhile, a study on the behavior after local buckling or fracture has not been conducted.

On the viewpoint mentioned above, the effects of the restriction of the axial deformation of H-shaped steel beams on the degradation behavior due to local buckling and fracture are investigated in this paper. On the front part, an experimental study of beam-column subassemblies to verify the differences of the strength degradation and the ultimate state between with and without the axial restriction of the beam is introduced. Further on the latter part, a numerical study by finite element method to reveal the degradation behavior with arbitrary axial deformation restriction is represented. Finally, the procedure to check whether the effect of axial deformation restriction should be considered with the complete collapse analysis of steel moment-resisting frames is proposed.

2. Cyclic loading test of beam-column subassemblies

2.1 Test specimen and loading procedure

Test specimen and loading equipment are shown in Fig. 1. The test specimen consists of a cold roll-formed steel box-column and a welded H-shaped steel beam, whose flanges are welded to through diaphragms inserted into the column.

Test parameters are width-to-thickness ratios of the beam, the presence or absence of weld access holes at the beam flange connections, and the presence or absence of the restriction of axial deformation of the beam. Three kinds of beams with deferent width-to-thickness ratios are used. Weld access holes are adopted for the beam flange connections except for group Cn. The effects of weld access holes will be confirmed by comparing the results between C and Cn. All groups are composed of the specimen with restriction of axial deformation of the beam (R) and the specimen without restriction (F). In Table 2, the mechanical properties of steel materials that are obtained by coupon tests are shown. The calculated strengths of the beams are shown in Table 1 using the measured plate thicknesses and yield strengths.

Beam end and column ends corresponding to the inflection points are connected to pin-joints, and the pin-joint at the beam end is supported by the loading column, as shown in Fig. 1. A horizontal force is applied to the loading beam by the hydraulic jack, according to the loading protocol shown in Fig. 2. The loading test is continued until significant strength degradation occurs due to fracture or local buckling except for the specimens of group Cn.



As shown in the dashed box column of Fig. 1, the pin-joint at the top of the loading column is fastened to the loading beam by high-strength bolts in case of specimens with the axial deformation restriction. On the contrary, linear sliders are installed between the pin-joint and the loading beam in case of specimens without the axial deformation restriction, as the top of the column can move to the longitudinal direction of the beam. Further, the lateral stiffening members (see Fig. 1) are settled for restraining lateral-torsional buckling of the beam of all specimens.

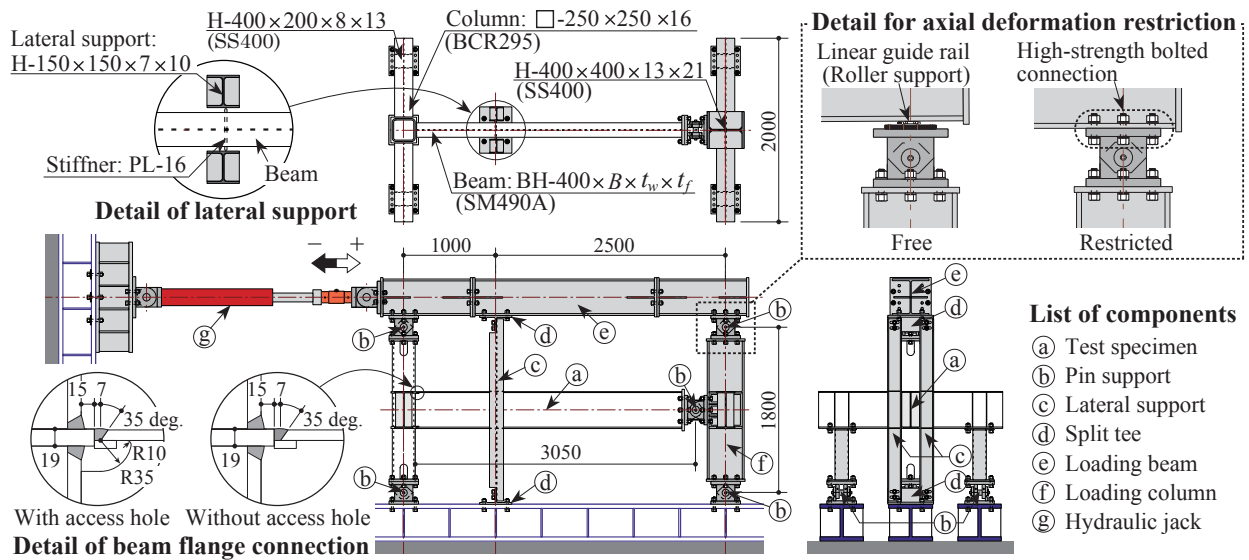


Fig. 1 – Test setup (unit: mm)

Table 1 – List of test specimen

Specimen	Test parameters				Calculated strengths		
	Sectional dimension of beam (Steel grade: SM490A)	Width-to-thickness ratio		Weld access holes	Restriction of axial deformation of beam	Yield moment M_v (kNm)	Full-plastic moment M_p (kNm)
		b/t_f	d/t_w				
A-F	H-400x160x9x12	6.67	41.8	With	Free	324	385
A-R					Restricted		
C-F	H-400x220x9x12	9.17	41.8	With	Free	418	482
C-R					Restricted		
Cn-F	H-400x220x9x12	9.17	41.8	No	Free	426	486
Cn-R					Restricted		
D-F	H-400x240x6x9	13.3	63.7	With	Free	366	397
D-R					Restricted		

Note: Strengths are calculated based on the pre-measured thicknesses and yield strengths in Table 2.

Table 2 – Mechanical properties of steel (unit: N/mm²)

Adapted specimen group	Flange		Web	
	Yield strength	Tensile strength	Yield strength	Tensile strength
A	356	523	388	551
C				
Cn	365	517	386	527
D	386	527	355	537

Note: Yield strengths are obtained by 0.2% offset method.

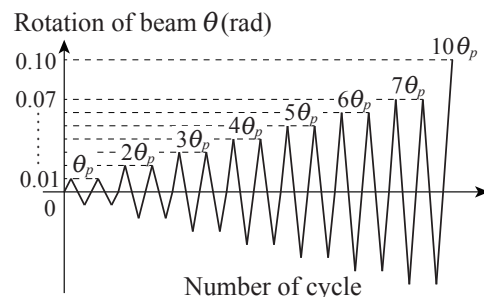


Fig. 2 – Loading protocol



2.2 Test results

Fig. 3 shows the relationships between bending moment M at the beam end and rotation θ of the beam. The vertical axis value is normalized by the full-plastic moment M_p shown in Table 1, and the horizontal axis value is normalized by the elastic rotation θ_p when the bending moment reaches the full-plastic moment M_p . In the figure, not only test results but also numerical results (FEA results) are illustrated, however, the numerical results are mentioned in the next chapter.

Regarding specimens of group A; a ductile crack like a hairline was observed at the toe of the weld access hole at the second cycle of $3\theta_p$ positive loading regardless of restriction of axial deformation of the beam. The crack penetrated through the thickness of the beam flange, and then the strength degradation began at the first cycle of $4\theta_p$ loading. During the second cycle of $4\theta_p$ positive loading, ductile fracture of the beam flange occurred and the strength decreased rapidly. The strength degradation of the specimen A-F was slightly faster than that of the specimen A-R, however, the difference of M - θ relationship could not be recognized clearly in visual.

Regarding specimens of group C and Cn; the strength degradation of all specimens of group C and Cn occurred due to local buckling at the first cycle of $3\theta_p$ loading. The strength degradation of the specimens with restriction is slower than without restriction, further, the negative slope of M - θ relationship of the specimen Cn-R could not be seen and the peak strengths were almost constant. In case of the specimen of group C, the ductile crack of the beam flange was observed at the first cycle of $4\theta_p$ negative loading, and then, the ductile fracture occurred at the second cycle of $5\theta_p$ negative loading. On the other hand, in case of the specimen of group Cn, the ductile fracture of the beam flange didn't occur.

Regarding specimens of group D; the strength degradation occurred due to local buckling at the first cycle of $2\theta_p$ loading, that was the earliest of all groups. In case of the specimen D-F, the ductile crack was observed at the toe of the weld access hole at the first cycle of $4\theta_p$ positive loading, however, the cracks didn't spread after then, instead, strength reduced gradually because of combination local buckling and lateral-torsional buckling. Meanwhile, in case of the specimen D-R, ductile crack was observed at the toe of the weld access hole at the first cycle of $3\theta_p$, and then the ductile fracture of the flange occurred at the first cycle of $7\theta_p$ positive loading.

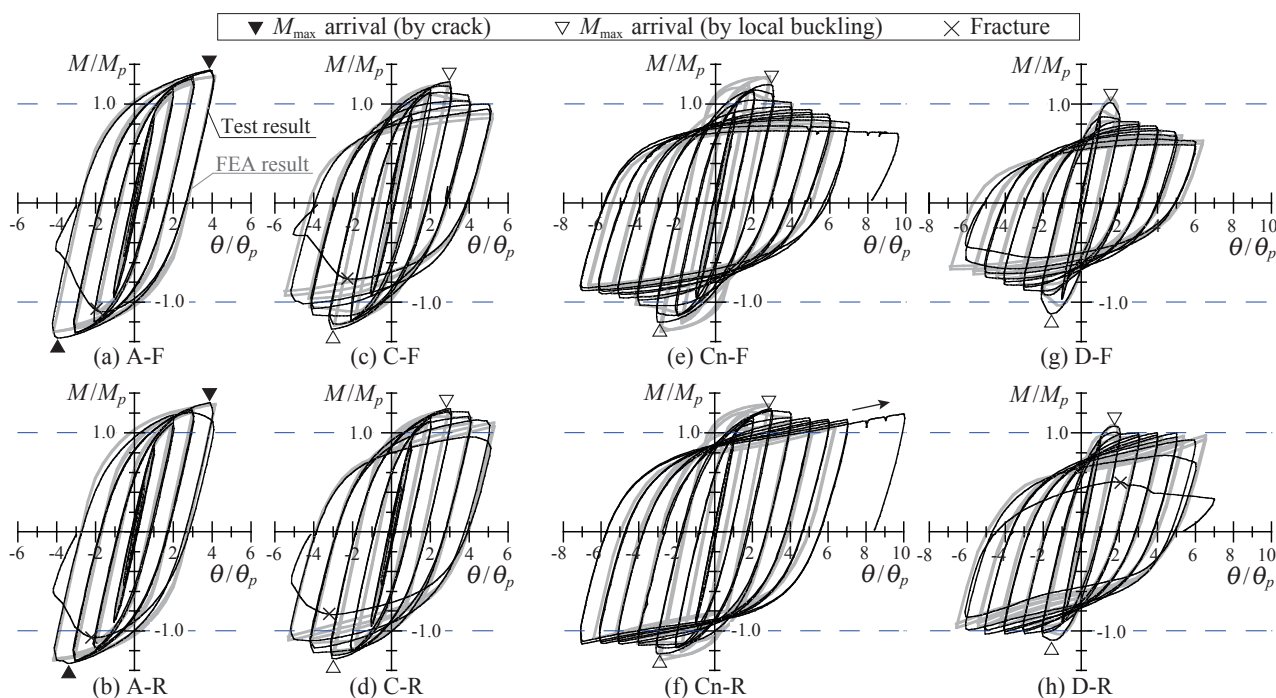


Fig. 3 – Bending moment M vs rotation θ relationship



The relationships between peak strength and plastic deformation capacity are shown in Fig. 4. The peak strength is the average of the positive and negative maximum bending moments at each cycle. Also, the plastic deformation capacity is defined by Eq. (1).

$$\eta_E = E_p / (M_p \theta_p) \tag{1}$$

Here, E_p is cumulative dissipation energy. In the figure, dashed circles mean the same cycle.

From Fig. 4, it is clarified that the plastic deformation capacities of group A are the smallest of all groups. Further, the difference in plastic deformation capacity between A-F and A-R is small because the local buckling didn't occur. On the contrary, the plastic deformation capacity of Cn-R and D-R (with the restriction) is slightly larger than that of Cn-F and D-F (without restriction) because the strength degradation becomes slower, as shown in Fig. 3, due to the axial restriction.

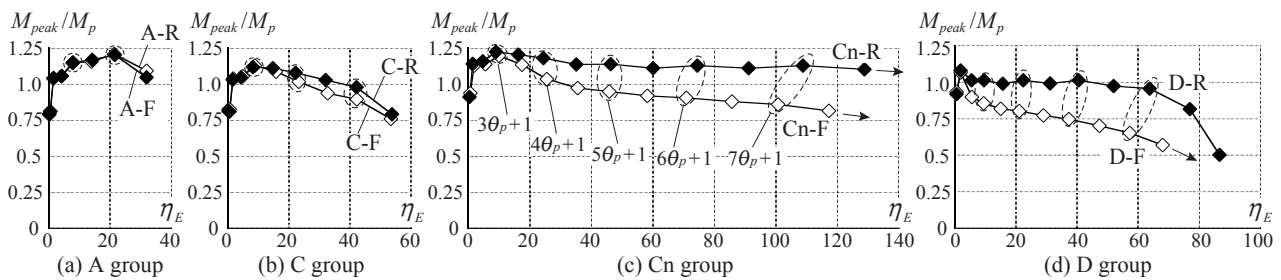


Fig. 4 – Cumulative plastic deformation capacity

The transition of out-of-plane deformation u of the beam flange of group Cn and D, on which the local buckling occurred dominantly, is shown in Fig. 5. The lateral axis of the figure means the number of loading cycles. The out-of-plane deformation of the beam flange, which is defined by the illustration in the box column of Fig. 5, was measured at the peak point and the unloading point. Through Fig. 5, out-of-plane deformations on the east side and west side of the compressive flange increase symmetrically. The residual deformations at the unloading point with the axial restriction are remarkably smaller than those without the restriction.

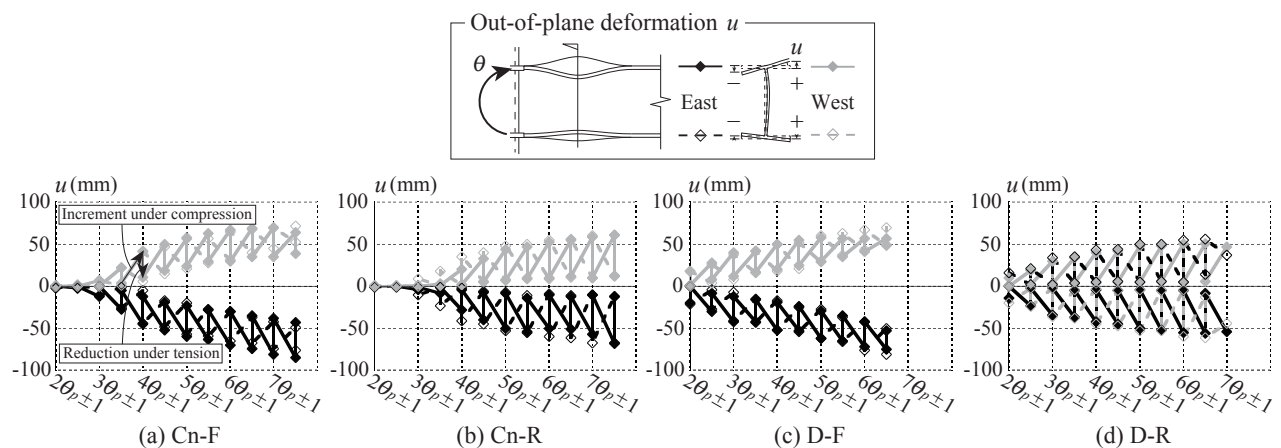


Fig. 5 – Out-of-plane deformation of beam flange

Fig 6 shows the relationship of the axial force and the rotation of the beam and Fig. 7 shows the relationship of the axial force and the axial deformation of the beam in case of group Cn and D. It is defined as tensile and shrinkage are positive in these figures. The black lines are represented test results, and the gray



lines are represented finite element analysis results explained in Chapter 3. On the other hand, the slopes of the dotted lines in Fig. 7, that is the rigidity of the axial restriction, are calculated by the following equation.

$$cal k_f = (1/k_{c1} + 1/k_{c2})^{-1} \tag{2}$$

Here, k_{c1} and k_{c2} are the elastic stiffnesses of the specimen column and the loading column, considered with flexural deformation and shear deformation of the columns, as shown in the box column of Fig. 8.

From Fig. 6 (a) and (c), even if the axial deformation of the beam was not restricted, the axial force slightly acts on the beam because the center of the pin-joint at the beam end stays away from the centerline of the loading column. However, the axial forces of the specimens without the axial restriction are quite smaller than that with the restriction. Further, from Fig. 6 (b) and (d), it is confirmed that the tensile axial forces increase rapidly after the bending moments reach the maximum values, and the compressive axial force occurs after the fracture at the beam flange. Also, it can be seen from Fig. 7 that the relationship between axial force and shrinkage of the specimen with axial restriction can be estimated by Eq. (2). Based on the discussions in this section, it is clarified that the strength degradation is restrained by the tensile axial force which increases due to the progress of local buckling of the beam with the axial deformation restriction.

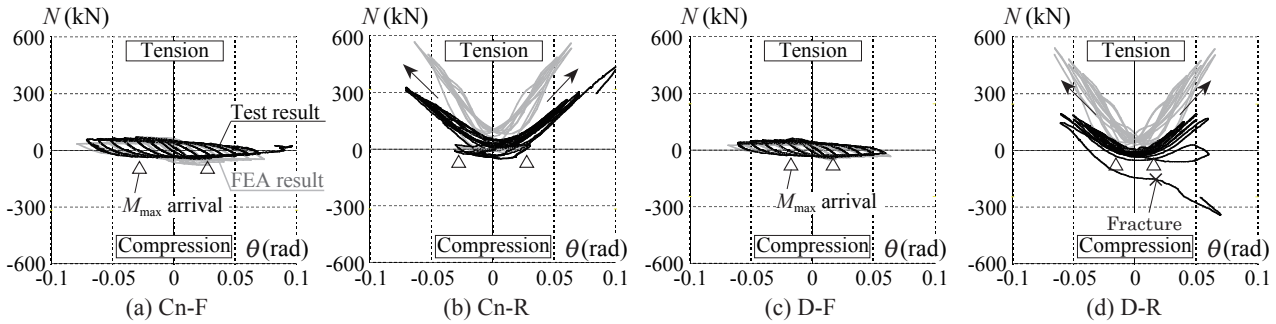


Fig. 6 – Axial force N on beam vs rotation θ relationship

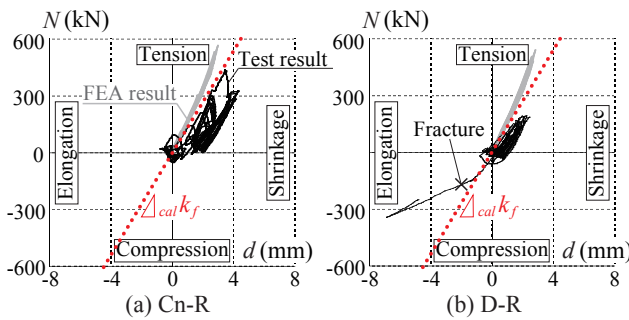


Fig. 7 – Axial force N on beam vs axial deformation d relationship

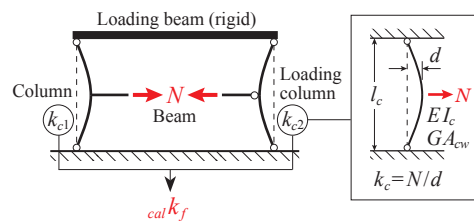


Fig. 8 – Calculation method of the axial deformation restriction $cal k_f$

3. Finite element analysis with varying axial restriction of beams

3.1 FEA with the same condition of experiment

Fig. 9 shows a numerical model for finite element analysis that consists of the box-column, the H-shaped beam, through diaphragms, stiffeners of the beam at the lateral supports, the loading column and the loading beam. A part of the model is made using C3D8R solid elements and the other parts using wire elements. The sizes of solid elements of the beam are 3 mm at the region of 250 mm (in case of A and C groups) or 300 mm (in case of Cn and D groups) far from the face of column, 7.5 mm at the region of 875 mm far from the



face of the column, and 20 mm at other region, respectively. Also, the size of solid elements of the panel zone and the diaphragms is determined as 20 mm. The sectional dimensions of wire elements are identical to that of the members in the loading test, and pin-joints at the ends of members are not modeled. The fillet welds whose sizes are the same as the thickness of the beam web at the beam flange-beam web joint and beam web-box column joint are considered. Further, the fillet weld whose size is 5 mm for settling the backing bar is also modeled. At the contact surfaces around the backing bars, the friction coefficient is assumed zero and rigid contact-separation is considered. At the other welded joints, elements are connected rigidly at the surface of each member.

Material properties of beam flange and beam web are determined based on the coupon test results shown in Fig. 10. Stiffeners and backing bars are assumed as the same material with beam web. The strengths of weld metals are assumed as 1.2 times that of the beam web. The other materials are modeled by only elastic properties. All elastic-plastic materials comply with Mises's yield condition and combined plastic flow rule. The parameters for flow rule are chosen to agree well with hysteresis curves between numerical results and test results. The initial imperfection of the beam whose out-of-plane deformation is 0.05% of the width of the beam flange is given based on the first buckling mode under simply compression.

The rigid bar for acting the bending moment is attached at both ends of the column. The whole model is supported at the center of the rigid bar and the loading column by a pin and a pin-roller, respectively. The rotation of the rigid bar, that is the story drift angle R , is provided based on the loading protocol in Fig. 2.

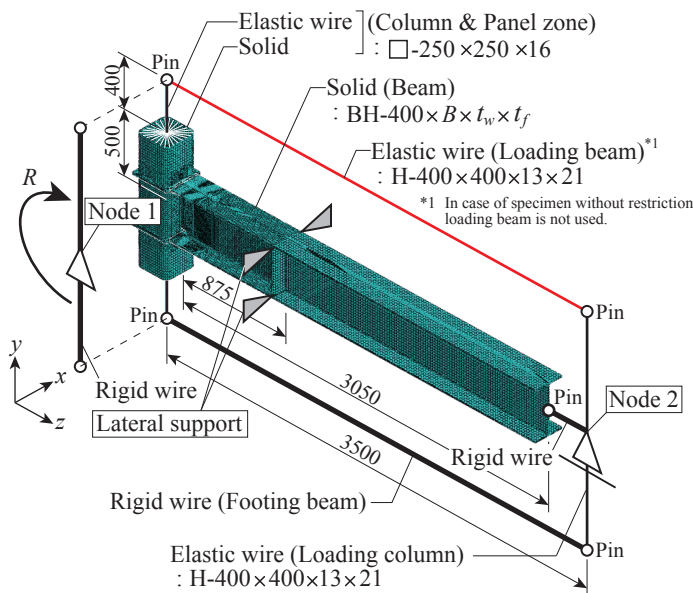
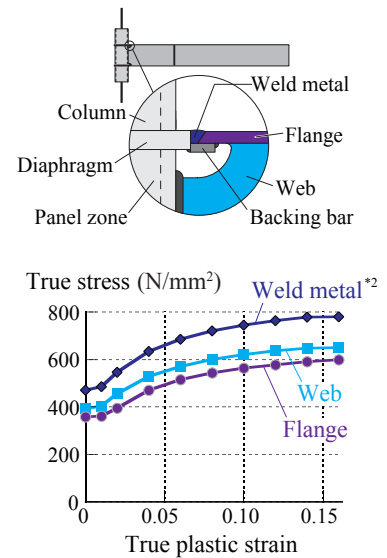


Fig. 9 – Outline of finite element analysis model for tracing the experiment (unit: mm)



*2 The true stress of weld metal is 1.2 times of the that of web

Fig. 10 – Material properties for finite element analysis

Comparisons between analysis results and test results are shown in Fig. 3, 6 and 7. From Fig. 3, it is confirmed that the bending moment and rotation relationships between analysis results and test results almost agree well with each other. However, differences in the strength degradation at the final cycle can be seen because the fracture of the beam flange was not considered in the finite element analysis. On the other hand, it can be identified that the axial force of the beam with the axial restriction by FEA is slightly larger than that by the test, as shown in Fig. 6 and 7. This would be caused that the out-of-plane deformation of the flange of the loading column and the endplate of the beam, further, the gaps in the pin-joints are ignored on the FEA.

To confirm the potential of development of the ductile fracture when the axial deformation is restricted or not, Fig. 11 illustrates the progress of the equivalent plastic strain at the toe of the weld access



hole where the crack initiation was observed in the loading test. Through Fig. 11, it is clarified that the differences of the equivalent plastic strain in groups A and C are quite small, however, the equivalent plastic strain of D-R specimen is larger than that of D-F. This is related that the fracture at the beam flange connection of D-R occurred only, and it would be deemed that the development of the ductile fracture becomes earlier in the only case of a beam with a large width-to-thickness ratio.

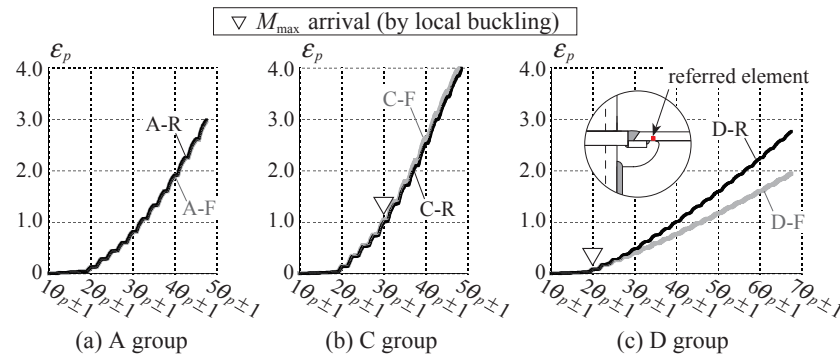


Fig. 11 – Comparison of equivalent plastic strain at the toe of weld access hole

3.2 FEA with various axial restriction of beams

In this section, parametric study varying the axial restriction of the beam is conducted to examine the effects of the axial restriction on the degradation behavior due to local buckling. The finite element analysis model, shown in Fig. 12, is modified as follows, compared with the model in Fig. 9. The first modification is adding an elastic wire element at the right side of the beam. The elastic stiffness (axial rigidity) k_f of the wire element, that is the axial restriction by adjacent members, is changed from 10 to 10^7 kN/m in every 10 times, so there are seven cases. The second modification is the loading procedure acting bending moment on the beam end. In Fig. 12, the columns and the loading beam are not modeled, instead a rigid bar connected to the centroids of the diaphragms to apply the bending moment. The other modeling procedures, for example, kind of elements, size of elements, material properties, yield condition, combined plastic flow rule, and loading protocol, are identical with the model in Fig. 9. The same sectional dimensions with the specimens of Cn and D groups are used for the FEA.

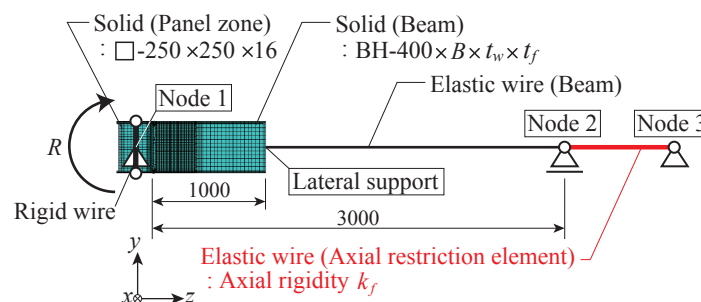


Fig. 12 – Outline of finite element analysis model for parametric study

Fig. 13(a) shows the maximum bending moment at each cycle in case of the specimen Cn. The results varying k_f from 10 to 10^3 kN/m are almost identical to each other and are considered as the degradation behavior without the axial restriction. On the other hand, the results varying k_f from 10^6 to 10^7 kN/m also agree with each other and deem as the behavior with full axial restriction. The greater the value of k_f increases between no restriction and full restriction, the more moderate the strength degradation becomes.

In this paper, the cycle when the bending moment with the minimum axial restriction reaches fully-plastic moment after achieving the maximum value is determined as the reference cycle, that is indicated the



circle in Fig. 13 (a), and the effect of the axial restriction on the strength degradation behavior is examined based on the peak strength at the reference cycle. Fig. 13 (b) shows the relationship between the peak strength at the reference cycle and the axial restriction of the beam. The lateral axis value is normalized by the axial stiffness k_b of the beam defined as Eq. (3).

$$k_b = EA/l \quad (3)$$

Here, A and l are the cross sectional area and the length of the beam respectively.

From Fig. 13 (b), the lines joining up with the peak strengths at the reference cycles can be categorized into three parts. At the low axial restriction part (in case k_f/k_b is less than 0.01), peak strengths are smaller than the other part as mentioned above, thus the effect of axial restriction on the degradation behavior does not appear. On the other hand, at the high axial restriction part (in case k_f/k_b is larger than 1.0), peak strengths are larger than the other part, thus the degradation of strength is restrained by the axial restriction. Note the peak strength almost keeps constant if the value of k_f/k_b gets larger 1.0.

For reference's sake, the calculated axial restrictions $_{cal}k_f$ of the loading test equipment are shown in Fig. 13 (b) and belong to the middle part of the axial restriction. The axial restriction in the steel moment-resisting frames is different from that of the loading test equipment. It would be recommended that the numerical model considering axial deformation of the beam is adopted for complete collapse analysis if the width-to-thickness ratio of the beam is large and the k_f/k_b is larger than 0.01 based on the real axial restriction.

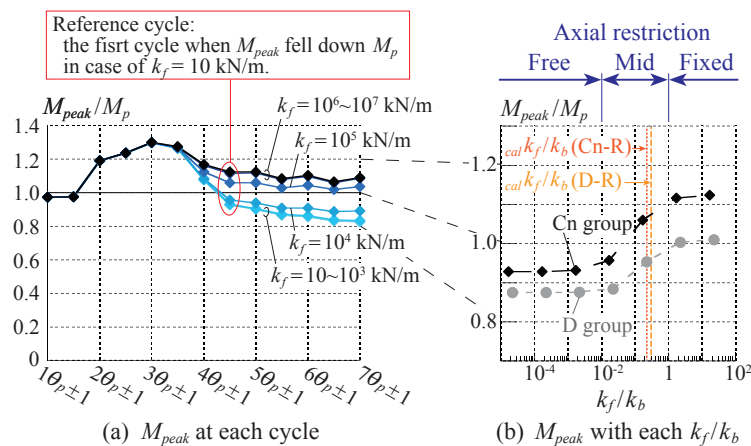


Fig. 13 – Transition of maximum bending moment at each cycle

4. Conclusions

In this paper, the cyclic loading test of beam-column assemblies was conducted to confirm the effect of axial restriction of the beam on the degradation behavior due to local buckling and fracture. Further, the differences in degradation behavior of the beam with the various axial deformation restriction were confirmed by the finite element analysis. The major findings from these studies are as follows.

1) From the cyclic loading test, it was verified that the strength degradation becomes slower and plastic deformation capacity becomes slightly larger by the axial restriction if local buckling dominantly occurred. The mitigation of degradation behavior would be caused by the tensile axial force on the beam, which developed along with the increment of out-of-plane deformation of the beam flange. On the other hand, if fracture at the beam flange dominantly occurred, it was confirmed that the difference of strength degradation between the presence and absence of the axial restriction was quite small.



2) From the finite element analysis, it was illustrated that the effect of axial restriction on degradation behavior was categorized into three parts, at which the axial deformation of the beam was free, fully fixed and intermediate of these two, respectively. As a result, it would be recommended, in complete collapse analysis of steel moment-resisting frames, to adopt a numerical model considering the axial deformation regarding the beam on which local buckling occurs dominantly if the ratio of axial restriction by the adjacent members to axial stiffness of the beam (k_f/k_b) is larger than 0.01.

References

- [1] Tada, M. et al. (2007): Plane pre-analytical simulation of collapse by hinge method for complete collapse specimen by large shaking table, *Steel Construction Engineering*, JSSC, **14** (56), 51-58 (in Japanese).
- [2] Horimoto, A., et al. (2007): Three dimensional analytical simulation of collapse by collaborative structural analysis for full-scale 4-story steel building, *Journal of Structural Engineering*, AIJ, **55B**, 277-283 (in Japanese).
- [3] D. G. Lignos, H. Krawinkler, A. S. Whittaker (2011): Prediction and validation of sidesway collapse of two scale models of a 4-story steel moment frame, *Earthquake Engineering & Structural Dynamics*, **40**, 807-825.
- [4] Mukaide, S., et al. (2013): Numerical analysis of collapsing behavior for multi-story steel moment frames considering strength degradation by local buckling, *Journal of Structural and Construction Engineering*, AIJ, **78** (685), 579-588 (in Japanese).
- [5] Wakatsuki, T., et al. (2013): Deformation concentration phenomena in lower part of frames on collapse by seismic analysis with fishbone-shaped frames, *Journal of Technology and Design*, AIJ, **19** (43), 945-950 (in Japanese).
- [6] Shugyo, M. and Shimazu, M. (2014): Elastoplastic seismic response analysis of a frame with lumped mass modeling by the fibered plastic hinge method, *Journal of Structural and Construction Engineering*, AIJ, **79** (696), 275-283 (in Japanese).
- [7] Kato, B., Akiyama, H., et al. (1978): Deformation characteristics of boxshaped steel members influenced by local buckling, *Transactions of the Architectural Institute of Japan*, 268, 71-76 (in Japanese).
- [8] Luis F. Ibarra, Ricardo A. Medina, Helmut Krawinkler (2005): Hysteretic models that incorporate strength and stiffness deterioration, *Earthquake Engineering & Structural Dynamics*, **34**, 1489-1511.
- [9] Kanao, I., et al. (2010): Primary studies on post-lateral buckling behavior of steel rigid frame subjected to horizontal force, *Journal of Structural and Construction Engineering*, AIJ, **75** (649), 643-649 (in Japanese).
- [10] Nakata, H. and Idota, H. (2010): Relations between slenderness of beam and k_D value in limit state design of steel structures, *Proceedings of Constructional Steel*, JSSC, **18**, 209-216, Tokyo, Japan (in Japanese).
- [11] Iga, H., Koetaka, Y., et al. (2015): Lateral buckling behavior of wide-flange beams with concrete floor slab subjected to cyclic bending moment, *8th International Conference on Behavior of Steel Structures in Seismic Areas*, 259-266, Shanghai, China.